Available online at www.sciencedirect.com
SCIENCE DIRECT®
Geochimica et Cosmochimica Acta 70 (2006) 687–696
Geochimica
www.elsevier.com/locate/gca

The solubility and speciation of molybdenum in water vapour at elevated temperatures and pressures: Implications for ore genesis

K.U. Rempel *, A.A. Migdisov, A.E. Williams-Jones

McGill University, 3450 University St., Montreal, Que., Canada H3A 2A7

Received 26 January 2005; accepted in revised form 26 September 2005

Abstract

The solubility of molybdenum trioxide in liquid–undersaturated water vapour has been investigated experimentally at 300, 320, and 360 °C and 39–154 bars. Results of these experiments show that the solubility of MoO_3 in water vapour is between 1 and 29 ppm, which is 19–20 orders of magnitude higher than the vapour pressure of MoO_3(g). Molybdenum solubility increases exponentially with f_{H_2O}, suggesting the formation of a gaseous hydrated complex of the type $MoO_3{\cdot}nH_2O$ by the reaction:

$$MoO_3(g) + nH_2O \Longleftrightarrow MoO_3 \cdot nH_2O(g) \quad (A.1)$$

The hydration number, n, is interpreted to have a value of 2.0 ± 1.0 at 300 °C, 2.4 ± 0.6 at 320 °C, and 3.1 ± 0.3 at 360 °C. Values of $\log K$ for this reaction are 18 ± 5 at 300 °C, 16 ± 3 at 320 °C, and 12 ± 1 at 360 °C. Comparison with data from the literature shows that the solubility of $MoO_3{\cdot}nH_2O$ increases non-linearly with increasing f_{H_2O}, and that the hydration number is equal to the slope of the tangent to a function inferred from a plot of $\log f_{MoO_3{\cdot}nH_2O}$ versus $\log f_{H_2O}$.The predominant species in water vapour at $f_{H_2O} \approx 1$ bar is $MoO_3{\cdot}H_2O$, whereas at the conditions of the present experiments it is $MoO_3{\cdot}2$–$3H_2O$. Calculations based on the solubility of MoO_3 in equilibrium with molybdenite at 600 °C and 500 bars, using average H_2O and total S fluxes of actively degassing volcanoes, with f_{O_2} and f_{S_2} controlled by the assemblage hematite–magnetite–pyrite, indicate that the vapour phase can transport sufficient Mo in about 115,000 years (within the life of geothermal systems) to form a deposit of 336 Mt, with an average grade of 0.087% Mo (e.g., the Endako Mo-porphyry deposit, Canada). This suggests that vapour-phase transport of Mo is far more important than previously thought and should be given further consideration in modelling the formation of porphyry molybdenum deposits.

1. Introduction

Although accepted models for the formation of porphyry Cu–Mo deposits have long assumed that the metals are transported by an aqueous liquid (e.g., Burnham, 1979; Eastoe, 1982), Henley and McNabb (1978) and Reynolds and Beane (1985) have proposed that the vapour phase may also play an important role in metal transport, as vapour commonly dominates the hydrothermal system in porphyry settings. This latter idea has recently gained support from studies reporting elevated concentrations of metals in vapour-rich fluid inclusions (Heinrich et al., 1992, 1999; Ulrich et al., 1999). For example, Ulrich et al. (1999) showed that at the Bajo de la Alumbrera Cu–Mo-Au porphyry deposit, Argentina, Cu and Mo concentrations in vapour-rich inclusions reach 1.2 wt% and 300 ppm, respectively, whereas their concentrations in the coexisting brine are 0.30 wt.% and 70 ppm, respectively. Significantly, metal-bearing condensates and sublimates collected from fumarolic gases are also commonly reported to contain high concentrations of metals, e.g., up to 0.8 ppm Mo in 700 °C fumaroles at Merapi volcano, Indonesia (Nadeau and Williams-Jones, unpublished data). Further support for the hypothesis of metal transport by vapour in hydrothermal systems is provided by experimental studies, which have shown that, at temperatures from

* Corresponding author.
E-mail address: kirstenr@eps.mcgill.ca (K.U. Rempel).

0016-7037/$ - see front matter © 2005 Elsevier Inc. All rights reserved.
doi:10.1016/j.gca.2005.09.013

280 to 360 °C and pressures up to 144 bars, metals such as Cu and Au can dissolve in H_2O–HCl vapours in concentrations approaching those required for ore-forming fluids (Archibald et al., 2001, 2002; Williams-Jones et al., 2002). The solubilities of these metals increase exponentially with water fugacity (f_{H_2O}), which led these researchers to conclude that the metals had formed gaseous hydrated complexes.

In this paper, we report the results of experiments designed to measure the solubility of molybdenum oxide in water vapour as a function of temperature and f_{H_2O}. We then go on to use these data to predict the speciation of Mo in water vapour and employ solubility data for these species to estimate the time required to form a Mo porphyry deposit under physicochemical conditions typical of porphyry Mo systems.

2. Experimental method

The experimental method employed in this study is based on that published by Migdisov and Williams-Jones (2005) for the SnO_2–HCl–H_2O system. Experiments were performed in autoclaves constructed of titanium alloy (Grade 2 ASTM B348), the inner surfaces of which were preconditioned with nitric acid to produce a protective layer of TiO_2. Before loading, autoclave volumes were measured by filling with 25 °C Nanopure water from a beaker and weighing the beaker before and after filling. These measured volumes were then used to calculate the water vapour pressure inside the autoclaves. As the vapour pressure of MoO_3 is negligible compared to that of H_2O, the total pressure of the system was assumed to be equal to that of water vapour.

Autoclaves were loaded with powdered molybdenum(VI) oxide (Alfa Aesar, 99.9995% purity), which was placed in open silica glass ampoules. Experiments buffered for f_{O_2} employed an additional ampoule of powdered MoO_2 (Alfa Aesar, 99% purity). The ampoules were supported inside the autoclaves by silica glass holders, which served to suspend the powdered molybdenum oxide above the solvent at the start of an experiment. The solvent consisted of between 2.0 and 10.0 mL of Nanopure water, which was pipetted into the bottom of the autoclave, and represented amounts calculated to produce dry vapour at the conditions of the experiment; water vapour pressures never approached liquid saturation. The experimental apparatus is shown schematically in Fig. 1.

For experiments conducted at 300 and 320 °C, autoclaves were heated in a Fisher Isotemp forced-draft oven (model 838F). A Barnstead Thermolyne muffle furnace (model 30400) was used for experiments at 360 °C. In order to reduce thermal gradients, autoclaves were placed inside aluminium boxes with wall thicknesses of 1.5 and 0.5 cm for the low-temperature and high-temperature experiments, respectively. At the completion of each experiment, the autoclaves were quenched in a cold water bath until room temperature was attained (less than 1 h).

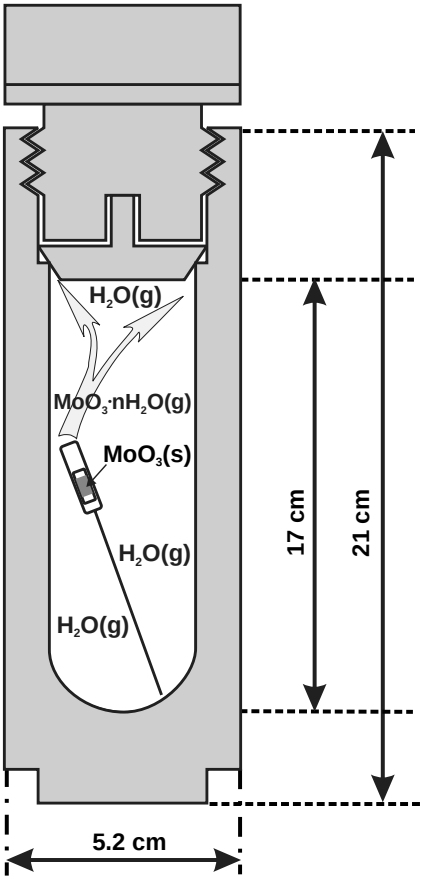

Fig. 1. Schematic diagram of the titanium autoclaves employed in the experiments. The autoclaves were constructed of Grade II ASTM B348 titanium alloy, and the interiors were preconditioned with nitric acid to provide a protective coating of TiO_2. The autoclaves are loaded with a silica holder containing a silica ampoule of MoO_3 or of MoO_2–MoO_3 for buffered experiments. At the experimental temperatures (illustrated here), all water is present as H_2O vapour and the predominant Mo species is of the form $MoO_3 \cdot nH_2O$(g).

After quenching, the autoclaves were opened, the silica glass holders and ampoules were removed, and 1 mL of hydrochloric acid (Optima grade, Fisher Scientific) was added to dissolve any precipitate on the autoclave walls. The walls were washed 50–60 times with 1 mL aliquots of the resulting solution to ensure that any Mo on the sides of the autoclave was collected. The condensate was pipetted into a clean plastic test tube, sealed, and weighed. Molybdenum concentrations in the condensates were analysed by ICP-MS; the detection limit was 0.1 ppb.

There are three potentially important sources of error in these experiments. The first is irreversible deposition of Mo on the cold parts of the autoclaves (the walls) due to temperature gradients in the ovens and would be evident as anomalously high Mo concentrations in the run condensates. The second source of error results from the partitioning of Mo from the vapour phase into the liquid during heating or quenching of the autoclaves and would also produce exceptionally high Mo concentrations (as Mo is much more soluble in the liquid than in the vapour). The third source of error arises from residual Mo on the autoclave

walls and was investigated by blank experiments. Irreversible transport of Mo onto the autoclave walls and partitioning into the liquid phase were evaluated by a series of kinetic experiments and by the amount of scatter in the data sets, respectively.

3. Results

A series of variable-time (kinetic) runs was conducted to estimate the amount of time needed for the system to reach equilibrium. These experiments were conducted at 320 °C and a constant water vapour pressure of about 100 bars, for durations of 1–14 days. At this temperature, equilibrium was reached in 6 days, after which Mo solubility was constant to ±16% (Fig. 2). This reproducibility indicates that errors due to irreversible deposition of Mo on the walls of the autoclaves and partitioning of Mo into the liquid were negligible. All subsequent experiments at 300 and 320 °C were conducted for periods of at least 12 days and those at 360 °C for at least 8 days.

To evaluate experimental error arising from residual Mo on the autoclave walls, which would result in anomalously high Mo concentrations, a set of five blank runs was also conducted. These experiments, which were not loaded with MoO_3 ampoules, were run at 320 °C and a water vapour pressure of about 100 bars, in previously used autoclaves. The run products had Mo concentrations between 0.5 and 1 ppm, which indicates that some Mo was transferred onto the autoclave walls during previous experiments and not completely removed during the cleaning process. In comparison, the condensates from solubility experiments conducted at the same P–T conditions had Mo concentrations an order of magnitude higher (7–19 ppm at 100–105 bars). The error arising from residual Mo on the autoclave walls is therefore considered to be minor.

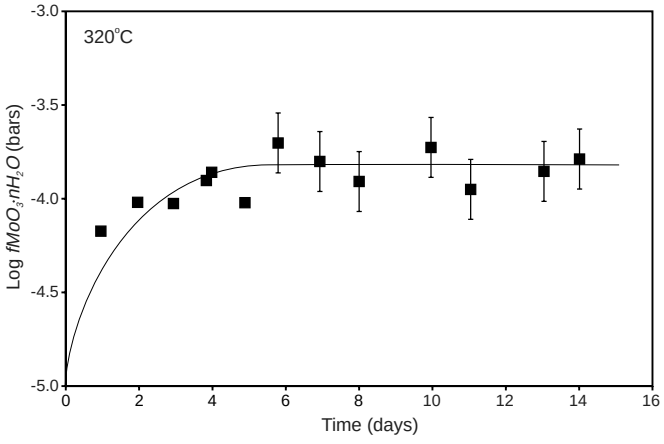

Fig. 2. Results of kinetic runs at 320 °C, showing the change in molybdenum concentration ($\log f_{MoO_3} \cdot nH_2O$) with time. Values of $\log f_{MoO_3} \cdot nH_2O$ were corrected for the Poynting factor, $\frac{V^o(P-1)}{RT}$. The solid line is a line of best fit to the experimental data and indicates that equilibrium was attained after 6 days. After this time, measured concentrations are within ±16% of the best-fit concentrations (error bars).

Three temperatures (300, 320, and 360 °C) were selected at which to investigate the solubility of Mo in water vapour. Twenty-seven experiments were conducted at 300 °C and 39–76 bars water vapour pressure (Table 1). At these conditions, the Mo concentrations of the run condensates were up to 17.9 ppm (1 ppm = 1 mg/L). Twenty-one experiments were conducted at 320 °C, with P_{H_2O} ranging from 57 to 105 bars (Table 2). The run products of these experiments had Mo concentrations up to 23.5 ppm. At 360 °C, 12 experiments were run for pressures between 62 and 154 bars, resulting in Mo concentrations up to 28.7 ppm (Table 3). The reproducibility of solubility measurements, calculated from a least-squares error analysis, is ±28% at 300 °C, ±16% at 320 °C, and ±10% at 360 °C. At all three of these temperatures, Mo concentrations increased with increasing fugacity of water vapour (f_{H_2O}; Figs. 3–5). The error inherent in the solubility data, however, does not permit an analysis of the dependence of Mo solubility on temperature, as the data show a nearly co-linear correlation of $\log f_{Mo}$ to $\log f_{H_2O}$ from 300 to 360 °C. The measurement of water vapour pressures is accurate to the third significant figure (i.e., ±0.1 bar) and, therefore, the error in these measurements is insignificant.

4. Discussion

4.1. Data treatment

As experimentally determined Mo fugacties are roughly twenty orders of magnitude higher than in the water-free system (10^{-24} bars at 320 °C, calculated using data from Pankratz, 1982; Fig. 6), it is evident that the solvent plays an important role in Mo solubility. The observed increase in f_{Mo} with f_{H_2O} (Figs. 3–5) shows that gaseous speciation of Mo is controlled by solvent–solute interactions. This interaction may involve the formation of a hydration shell or Mo–OH bonds, but these two types of interactions cannot be distinguished by the method employed. The experimental method also does not allow for distinction between monomeric and polymeric species (i.e., a species such as $Mo_2O_6 \cdot nH_2O$ is indistinguishable from $MoO_3 \cdot nH_2O$). Owing to the relatively low concentration of Mo in water vapour at our experimental conditions, we have, in the following discussion, assumed that the predominant species is a monomeric hydrated complex of the form $MoO_3 \cdot nH_2O(g)$, which is produced by the reaction

$$MoO_3(s) + nH_2O(g) \Longleftrightarrow MoO_3 \cdot nH_2O(g) \quad (1)$$

The hydration number, n, is statistical in nature and may vary with both temperature and pressure, but as a first approximation we can assume that n is constant over the range of pressures investigated in this study and thus varies only with temperature. This allows us to regard reaction (1) as a stoichiometric reaction and thereby determine the hydration number from the equilibrium constant for that reaction, as discussed below.

Table 1
Results of solubility experiments at 300 °C

P_{H_2O} (bars)	φH_2O	$\log f_{H_2O}$ (bars)	H_2O (10^{-1} mol)	[Mo] (ppm)	Mo (10^{-7} mol)	$\log f_{Mo}$, (bars)	PF
39.1	0.90	1.55	0.83	6.8	1.06	−4.30	0.024
48.1	0.88	1.63	0.94	7.7	1.36	−4.16	0.030
50.5	0.88	1.65	1.06	2.0	0.41	−4.71	0.032
52.6	0.87	1.66	1.11	2.5	0.52	−4.61	0.033
54.5	0.87	1.67	1.11	7.4	1.55	−4.12	0.034
55.3	0.86	1.68	1.11	2.9	0.59	−4.53	0.035
57.4	0.86	1.69	1.17	10.1	2.21	−3.96	0.036
59.7	0.85	1.71	1.22	7.7	1.75	−4.07	0.038
61.0	0.85	1.71	1.39	4.1	1.08	−4.32	0.039
62.0	0.85	1.72	1.28	10.2	2.45	−3.92	0.039
63.1	0.84	1.73	1.33	8.5	2.12	−4.00	0.040
63.4	0.84	1.73	1.39	7.5	1.94	−4.05	0.040
64.2	0.84	1.73	1.33	3.2	0.79	−4.42	0.041
65.2	0.84	1.74	1.39	3.2	0.83	−4.41	0.041
65.2	0.84	1.74	1.44	7.5	2.03	−4.04	0.041
66.1	0.84	1.74	1.44	9.0	2.43	−3.95	0.042
67.1	0.83	1.75	1.50	16.3	4.59	−3.69	0.042
68.0	0.83	1.75	1.50	4.7	1.33	−4.22	0.043
68.9	0.83	1.76	1.56	5.0	1.45	−4.19	0.044
69.3	0.83	1.76	1.56	5.4	1.58	−4.15	0.044
71.2	0.82	1.77	1.78	1.3	0.43	−4.77	0.045
71.4	0.82	1.77	1.61	12.1	3.65	−3.79	0.045
73.8	0.82	1.78	1.61	7.5	2.26	−3.98	0.047
73.9	0.82	1.78	1.67	4.3	1.33	−4.23	0.047
74.5	0.81	1.78	1.72	17.9	5.77	−3.60	0.047
75.5	0.81	1.79	1.67	5.9	1.86	−4.08	0.048
76.3	0.81	1.79	1.78	13.5	4.51	−3.71	0.048

P_{H_2O} is the water vapour pressure in each autoclave, determined from the P–V–T properties of water; φH_2O is the fugacity coefficient for H_2O; $\log f_{H_2O}$ is the log fugacity of H_2O(g), calculated as $(P_{H_2O})(\varphi H_2O)$; H_2O is the total mass of H_2O, in moles, introduced into the system; [Mo] is the concentration of Mo, in ppm, measured in the condensate; Mo is the total mass of Mo, in moles, transported in the vapour; $\log f_{Mo}$ is the fugacity of $MoO_3{\cdot}nH_2O$(g), assuming ideal behaviour; PF is the Poynting factor, $\frac{V^o(P-1)}{RT}$.

Table 2
Results of solubility experiments at 320 °C

P_{H_2O} (bars)	φH_2O	$\log f_{H_2O}$ (bars)	H_2O (10^{-1} mol)	[Mo] (ppm)	Mo (10^{-7} mol)	$\log f_{Mo}$ (bars)	PF
57.1	0.88	1.70	1.11	6.6	1.37	−4.15	0.035
68.4	0.85	1.77	1.39	11.1	2.88	−3.85	0.042
68.7	0.85	1.77	1.39	7.3	1.90	−4.03	0.042
68.9	0.85	1.77	1.39	8.2	2.15	−3.97	0.042
74.1	0.84	1.79	1.50	4.4	1.23	−4.22	0.045
78.4	0.83	1.81	1.67	9.8	3.08	−3.84	0.048
79.9	0.83	1.82	1.67	9.2	2.89	−3.86	0.049
84.6	0.82	1.84	1.83	5.5	1.89	−4.06	0.052
87.4	0.81	1.85	1.94	11.8	4.29	−3.72	0.054
88.1	0.81	1.85	1.94	8.5	3.11	−3.85	0.054
91.9	0.80	1.87	2.06	10.2	3.94	−3.75	0.056
95.0	0.79	1.88	2.22	23.5	9.80	−3.38	0.058
96.3	0.79	1.88	2.22	6.4	2.68	−3.93	0.059
97.3	0.79	1.88	2.22	9.2	3.84	−3.77	0.060
97.3	0.79	1.88	2.22	11.9	4.94	−3.66	0.060
101.3	0.78	1.90	2.50	7.4	3.45	−3.85	0.062
101.6	0.78	1.90	2.50	13.9	6.54	−3.58	0.062
102.1	0.78	1.90	2.50	15.3	7.17	−3.53	0.063
103.5	0.77	1.90	2.50	8.7	4.08	−3.77	0.064
105.2	0.77	1.91	2.78	19.1	9.95	−3.42	0.065
105.4	0.77	1.91	2.50	8.2	3.86	−3.79	0.065

See caption of Table 1 for further explanation.

In the calculations that follow, it is assumed that the partial pressure of $MoO_3{\cdot}nH_2O$ is negligible compared to that of H_2O, and thus the total vapour pressure of the system is equal to the partial pressure of water vapour (P_{H_2O}). As the thermodynamic properties of water are well described, water is treated as a real gas, and thus

Table 3
Results of solubility experiments at 360 °C

P_{H_2O} (bars)	φH_2O	$\log f_{H_2O}$ (bars)	H_2O (10^{-1} mol)	[Mo] (ppm)	Mo (10^{-7} mol)	$\log f_{Mo}$ (bars)	PF
62.0	0.90	1.75	1.11	5.1	1.07	−4.22	0.035
89.5	0.85	1.88	1.67	12.5	3.90	−3.68	0.051
89.9	0.85	1.88	1.67	8.0	2.51	−3.87	0.052
101.9	0.83	1.93	2.22	8.0	3.35	−3.81	0.059
107.5	0.82	1.95	2.22	11.3	4.71	−3.64	0.062
107.7	0.82	1.95	2.22	16.7	6.97	−3.47	0.062
130.2	0.78	2.01	2.78	13.7	7.13	−3.48	0.075
130.3	0.78	2.01	2.78	18.7	9.73	−3.34	0.075
139.9	0.77	2.03	3.33	17.9	11.21	−3.33	0.081
146.0	0.75	2.04	3.33	17.5	10.94	−3.32	0.084
146.0	0.75	2.04	3.33	15.2	9.53	−3.38	0.084
153.7	0.74	2.06	3.89	25.6	18.68	−3.13	0.089
153.8	0.74	2.06	3.89	28.7	20.94	−3.08	0.089

See caption of Table 1 for further explanation.

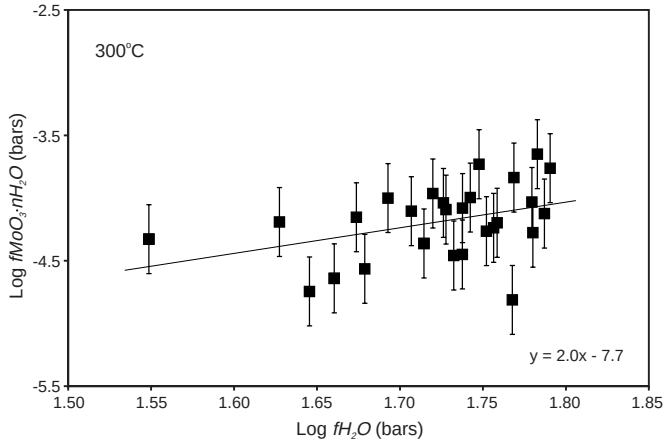

Fig. 3. A plot of $\log f_{MoO_3 \cdot nH_2O}$ corrected for the Poynting factor, $\frac{V^o(P-1)}{RT}$, versus $\log f_{H_2O}$, showing the results of solubility experiments conducted at 300 °C. The slope of the best fit line ($y = 2.0x - 7.7$) corresponds to the hydration number, which in this case is 2.0 ± 1.0. Error bars were determined by least-squares error analysis and represent a reproducibility of ±28%.

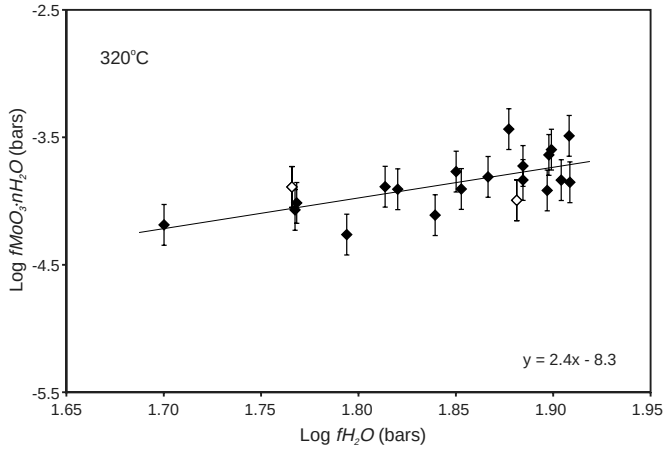

Fig. 4. A plot of $\log f_{MoO_3 \cdot nH_2O}$ corrected for the Poynting factor, $\frac{V^o(P-1)}{RT}$, versus $\log f_{H_2O}$, showing the results of solubility experiments conducted at 320 °C. Open and closed diamonds represent buffered and unbuffered experiments, respectively. The slope of the best fit line ($y = 2.4x - 8.3$) corresponds to the hydration number, which in this case is 2.4 ± 0.6. Error bars were determined by least-squares error analysis and represent a reproducibility of ±16%.

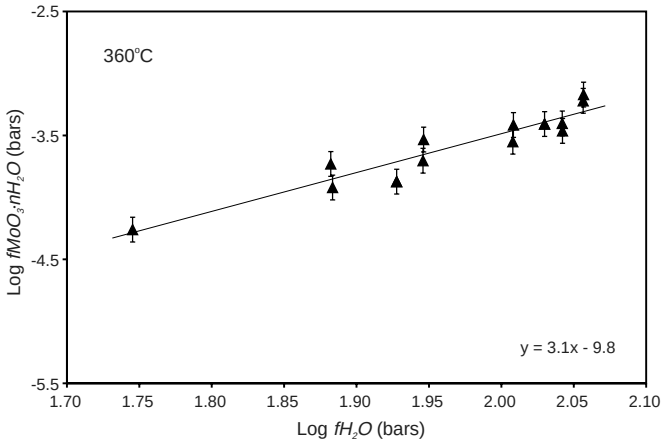

Fig. 5. A plot of $\log f_{MoO_3 \cdot nH_2O}$ corrected for the Poynting factor, $\frac{V^o(P-1)}{RT}$, versus $\log f_{H_2O}$, showing the results of solubility experiments conducted at 360 °C. The slope of the best fit line ($y = 3.1x - 9.8$) corresponds to the hydration number, which in this case is 3.1 ± 0.3. Error bars were determined by least-squares error analysis and represent a reproducibility of ±10%.

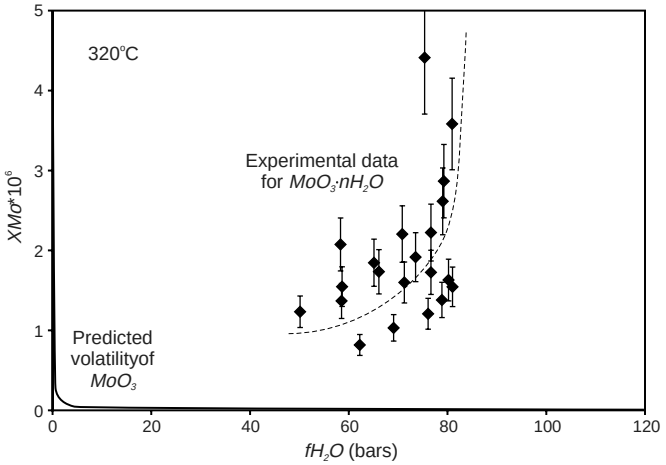

Fig. 6. A plot of $X_{MoO_3 \cdot nH_2O}$ versus f_{H_2O} for dry and water-bearing systems at 320 °C. Diamonds represent experimentally determined data points, the dashed curve is an exponential curve of best fit to the experimental data, and the solid curve is the mole fraction of MoO_3 predicted from volatility calculations (Pankratz, 1982), which is infinite in a pure MoO_3 gas, but decreases to near zero when H_2O gas is added.

$$f_{H_2O} = (\varphi_{H_2O})(P_{H_2O}), \quad (2)$$

where φ_{H_2O} is the fugacity coefficient of H_2O and accounts for the non-ideal behaviour of the gas (Anderson and Crerar, 1993). Fugacity coefficients and water vapour pressures were calculated using the equation of state of Kestin et al. (1984). The fugacity of $MoO_3{\cdot}nH_2O$ was calculated using the Mo concentrations of the run products, which were converted to mole fractions ($X_{MoO_3{\cdot}nH_2O}$) and then to fugacities ($f_{MoO_3{\cdot}nH_2O}$). The mole fraction of the gaseous Mo hydrate is given by the number of moles of the hydrate over the number of moles of H_2O:

$$X_{MoO_3{\cdot}nH_2O} \cong \frac{M_{MoO_3{\cdot}nH_2O}}{M_{H_2O}}, \quad (3)$$

where M_i is the number of moles of component i, and was used to estimate $f_{MoO_3{\cdot}nH_2O}$, assuming that the species is an ideal gas ($\varphi_{MoO_3{\cdot}nH_2O} = 1$). Thus

$$f_{MoO_3{\cdot}nH_2O} = P_{MoO_3{\cdot}nH_2O} = (X_{MoO_3{\cdot}nH_2O})(P_{H_2O}). \quad (4)$$

As discussed in Migdisov and Williams-Jones (2005), the hydration number (n) for the product of reaction (1) can be determined by differentiating the expression for the logarithm of the equilibrium constant ($\log K$). However, as the formation of the hydrated complex involves the reaction of MoO_3(s) to form MoO_3(g), $\log K$ is dependent on the total pressure of the system ($P_{H_2O} = P_{total}$). In order to convert this heterogeneous system into one that is independent of pressure, i.e., MoO_3(s) instead of MoO_3(g), reaction (1) was considered to represent the following two consecutive reactions:

$$MoO_3(s) \Longleftrightarrow MoO_3(g) \quad (5)$$

$$MoO_3(g) + nH_2O(g) \Longleftrightarrow MoO_3 \cdot nH_2O(g) \quad (6)$$

where the latter expression is a homogeneous gas-phase reaction, and thus, for ideal gases, is independent of pressure. The equilibrium constant ($\log K_5$) for reaction (5) is dependent on the total pressure of the system as follows:

$$\left(\frac{\partial \log K_5}{\partial \log P_{total}}\right)_{(T)} = \int_{P_1}^{P_2} \frac{V^o}{RT}\,dP \cong \frac{V^o(P_2 - P_1)}{RT}, \quad (7)$$

where V^o is the molar volume of MoO_3(s) (3.056 J bar^{-1}; Robie et al., 1966) and $\frac{V^o(P-1)}{RT}$ is the Poynting pressure correction (Sandler, 1989). The fugacity of MoO_3(g) must therefore be corrected as follows:

$$\log f MoO_{3(P,T)} = \log f MoO_{3(P=1,T)} + \frac{V^o(P-1)}{RT}, \quad (8)$$

where f_{MoO_3} is constant at constant pressure, and the standard state is 1 bar and the temperature of interest. The equilibrium constant for reaction (6) is thus given by the following expression:

$$\begin{aligned}\log K_6 &= \log f MoO_3 \cdot nH_2O - n \log f H_2O \\ &\quad - \log f MoO_{3(P,T)} \\ &= \left(\log f MoO_3 \cdot nH_2O - \frac{V^o(P-1)}{RT}\right) \\ &\quad - n \log f H_2O - \log f MoO_{3(P=1,T)}. \end{aligned} \quad (9)$$

Differentiation of expression (9) with respect to f_{H_2O} at constant temperature yields

$$\left(\frac{\partial \log f MoO_3 \cdot nH_2O - \frac{V^o(P-1)}{RT}}{\partial \log f H_2O}\right)_T = n. \quad (10)$$

From Eq. (10), it follows that the hydration number n is given by the slope of the experimentally determined values of $\log f_{MoO_3{\cdot}nH_2O} - \frac{V^o(P-1)}{RT}$ plotted as a function of $\log f_{H_2O}$ at constant temperature (Figs. 3–5). The hydration number so determined is 2.0 ± 1.0 at 300 °C, 2.4 ± 0.6 at 320 °C, and 3.1 ± 0.3 at 360 °C. These data suggest that the hydration number increases with increasing temperature, but given the calculated errors, n can only be reported reliably as being between 2 and 3 for temperatures from 300 to 360 °C. Logarithms of the equilibrium constants for reaction (6) were calculated for each isotherm using experimentally determined fugacities of $MoO_3{\cdot}nH_2O$ and H_2O (with $f_{MoO_3(g)}$ calculated using data from Pankratz, 1982) and equalled 18 ± 5, 16 ± 3, and 12 ± 1 for 300 °C ($n = 2.0 \pm 1.0$), 320 °C ($n = 2.4 \pm 0.6$), and 360 °C ($n = 3.1 \pm 0.3$), respectively.

Molybdenum commonly speciates as Mo(IV) and Mo(VI), but the fugacity of Mo(VI) trioxide in a dry system is roughly 15 orders of magnitude greater than that of Mo(IV) dioxide (calculated using data from Pankratz, 1982), and thus hydrated Mo(VI) trioxide is likely the predominant gaseous species in water vapour. To test this hypothesis, two experimental runs at 320 °C and near-saturated water vapour pressure were held at a constant oxidation state with a MoO_2–MoO_3 buffer. Separate sample ampoules and holders were used for MoO_2 and MoO_3, and care was taken to ensure that no pre-run cross-contamination occurred between the two. The Mo concentrations of the condensed water from these runs were identical, within experimental error, to those of the non-buffered runs at 320 °C (Fig. 4), confirming that the predominant gaseous Mo species at the conditions of the experiments was a molybdenum(VI) trioxide hydrate. Post-run XRD analysis of the MoO_2 and MoO_3 ampoules showed that while no MoO_3 was reduced to MoO_2, MoO_2 was partially oxidized to MoO_3, indicating that the excess oxygen in the system was consumed. The oxygen fugacity was thus effectively buffered at the MoO_2–MoO_3 boundary (1×10^{-22} bars).

4.2. Comparison with previous studies

Early experimental studies showed that the vapour pressure of Mo increases with increasing f_{H_2O} (Table 4; Millner and Neugenbauer, 1949; Elliott, 1952; Glemser and von Haeseler, 1962; Sardi, 1963; Belton and Jordan, 1965; Buiten, 1968). With the exception of Elliott (1952), whose experiments were conducted in sealed silica tubes at 60–210 bars, these studies employed a transpiration technique, which involved measurement of the mass of Mo trioxide precipitated at a pressure of 1 bar from a stream of water

Table 4
Results of previous studies of the solubility of Mo in water vapour, listed in order of increasing temperature, where log*fMo* refers to the logarithm of the fugacity of the predicted gaseous Mo species in bars

T (°C)	f_{H_2O} (bars)	$\log f_{Mo}$ (bars)	Predicted species	Reference
400–500	1	−5.8 to −4.6	$MoO_2(OH)_2$	Buiten (1968)
500	60–210	−3.5 to −3.0	$MoO_3{\cdot}H_2O$	Elliott (1952)
600–690	0.03–1	−3.4 to −1.7	$MoO_2(OH)_2$	Glemser and von Haeseler (1962)
450–730	1	Not reported	None	Sardi (1963)
600–700	1	−3.8 to −2.7	$MoO_3{\cdot}H_2O$	Millner and Neugenbauer (1949)
1200–1500	0.04–0.5	−4.8 to −3.0	$MoO_3{\cdot}H_2O$	Belton and Jordan (1965)

The data of Millner and Neugenbauer (1949) and Elliott (1963) do not represent equilibrium, and the data of Belton and Jordan (1965) were determined for Mo(s), so these data cannot be directly compared.

vapour passed over a Mo-bearing solid. The solid employed in these experiments was MoO_3, except for those of Belton and Jordan (1965), who used Mo metal. Glemser and von Haeseler (1962) concluded that the increased vapour pressure of molybdenum was due to the formation of the species $MoO_2(OH)_2(g)$, as did Buiten (1968). By contrast, Belton and Jordan (1965) interpreted the molybdenum gas species to be $MoO_3{\cdot}H_2O$ and concluded that it formed by the reaction

$$Mo(s) + 4H_2O(g) = MoO_3 \cdot H_2O(g) + 3H_2(g) \qquad (11)$$

If, however, the data of Glemser and von Haeseler (1962) are re-analysed, assuming formation of $MoO_3{\cdot}nH_2O(g)$, the hydration number obtained is 0.95–1.0, i.e., their data also predict formation of the species $MoO_3{\cdot}H_2O$.

The experimental data of Belton and Jordan (1965), Glemser and von Haeseler (1962), and Buiten (1968) were used to provide the thermodynamic data reported in the JANAF Tables (Chase, 1998) for an ideal gas species referred to as molybdic acid (H_2MoO_4). However, as the species was interpreted by the experimental studies to be either $MoO_2(OH)_2$ or $MoO_3{\cdot}H_2O$, for the purposes of comparison we will refer to the species in the JANAF Tables as $MoO_3{\cdot}H_2O$.

In order to compare our results with those of earlier studies, which were conducted at $f_{H_2O} \leqslant 1$ bar (Buiten, 1968; Glemser and von Haeseler, 1962), we extrapolated our data linearly to 1 bar (Figs. 7–9). We did not make comparisons to the data of Belton and Jordan (1965), because they relate to a different speciation reaction, or to those of Millner and Neugenbauer (1949) and Elliott (1952), because these two data sets do not reflect equilibrium. Errors in the extrapolation of our data were limited by restricting the extrapolation to data collected at 360 °C, which had the least amount of scatter. The extrapolation was done by linearly regressing the data collected at 360 °C to a water fugacity of 1 bar, as illustrated in Fig. 7.

The fugacity of $MoO_3{\cdot}3.1H_2O$ predicted at 1 bar by extrapolation of our data is orders of magnitude lower than the fugacity of $MoO_3{\cdot}H_2O$ determined by Glemser and von Haeseler (1962) and Buiten (1968), illustrating that Mo speciation at 360 °C is dominated by $MoO_3{\cdot}H_2O$ at pressures below about 1.5 bars, but that $MoO_3{\cdot}3.1H_2O$ is

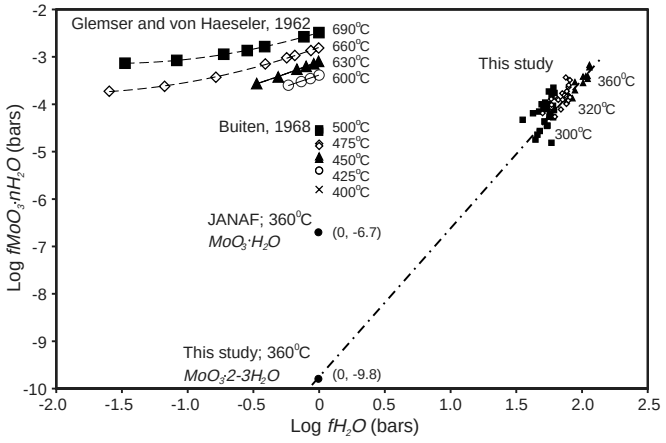

Fig. 7. A plot of $\log f_{MoO_3{\cdot}nH_2O}$ versus $\log f_{H_2O}$ comparing the data reported by Glemser and von Haeseler (1962), Buiten (1968), and this study, and data calculated from the JANAF Tables (Chase, 1998). The dash-dot line represents the linear regression of our 360 °C data, and the coordinates (0, −6.7) and (0, -9.8 ± 0.6) represent the values of $\log f_{MoO_3{\cdot}nH_2O}$ at 1 bar and 360 °C calculated from the JANAF Tables ($n = 1$) and regressed from our data ($n = 3.1 \pm 0.3$), respectively. The equations for polynomial curves of best fit for data from Glemser and von Haeseler (1962; dashed) are $y = 0.3x^2 + 1.0x - 2.8$ and $y = 0.3x^2 + 0.8x - 2.5$ for 660 and 690 °C, respectively, where y is $\log f_{H_2O}$ and x is $\log f_{MoO_3{\cdot}nH_2O}$. Because fewer data are available for 600 and 630 °C, these data were fitted to linear functions (solid), the equations of which are $y = 1.0x - 3.4$ and $y = 1.0x - 3.1$, respectively.

the dominant species above this pressure (Fig. 8). In light of the increase in hydration number with increasing f_{H_2O} observed in this study (from 2.0 ± 1.0 at 300 °C and 39–76 bars, to 2.4 ± 0.6 at 320 °C and 57–105 bars, and to 3.1 ± 0.3 at 360 °C and 62–154 bars), we propose that rather than changing abruptly from 1 to ~3 at $P \approx 1.5$ bars, the hydration number changes continuously with increasing f_{H_2O}. A similar conclusion can be drawn from the data of Glemser and von Haeseler (1962), illustrated in Fig. 7. Non-integral hydration numbers (e.g., $n = 2.4$) represent a combination of monohydrate and trihydrate species, the relative proportions of which change with changing $\log f_{H_2O}$. The trendlines for the $MoO_3{\cdot}H_2O$ and $MoO_3{\cdot}3.1$-H_2O data sets are therefore interpreted to represent tangents at 1 and ~100 bars to a hypothetical exponential function (the sum of the fugacities of all Mo species), which describes the variation of $\log f_{MoO_3{\cdot}nH_2O}$ with $\log f_{H_2O}$.

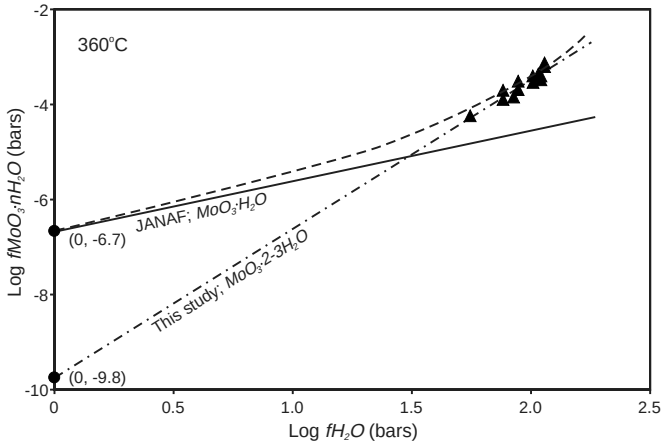

Fig. 8. A plot of $\log f_{MoO_3 \cdot nH_2O}$ versus $\log f_{H_2O}$ comparing the regressed trendline (dash-dot) fitted to our 360 °C data for pressures between 1 and 154 bars (triangles) with a trendline (solid) representing values for $\log f_{MoO_3 \cdot nH_2O}$ calculated from the JANAF Tables (Chase, 1998) for the same range of pressure. The two trendlines are interpreted to represent tangents at 1 and 100 bars to a hypothetical exponential function (dashed), which is considered to reconcile our results with those of earlier experiments. The coordinates (0, −6.7) and (0, −9.8) represent the fugacity of $MoO_3 \cdot H_2O$ and $MoO_3 \cdot 2–3H_2O$, respectively, at 1 bar, indicating that linear extrapolation of our data underestimates the fugacity of $MoO_3 \cdot nH_2O$ by three orders of magnitude.

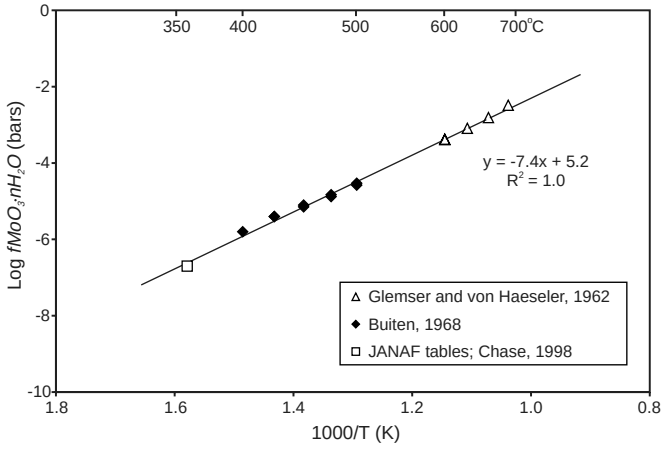

Fig. 9. Variation of $\log f_{MoO_3 \cdot nH_2O}$ with temperature (1000/T, K) at 1 bar. The datum at 360 °C was calculated from thermodynamic data in the JANAF tables, whereas the other data represent results of experiments conducted at $f_{H_2O} = 1$ bar. The equation of the line of best fit to all points (solid line) is $y = -7.4x + 5.2$.

The effect of temperature on $f_{MoO_3 \cdot nH_2O}$ could not be satisfactorily analysed from the results of our experiments because of the narrow interval of temperature investigated. However, inspection of the data for 1 bar from previous experimental studies shows clearly that $f_{MoO_3 \cdot nH_2O}$ also increases with temperature (Fig. 7). Furthermore, $f_{MoO_3 \cdot H_2O}$ decreases linearly with reciprocal temperature (Fig. 9). Whether the hydration number also changes with temperature is far less certain, although the flattening with increasing temperature of the slopes of the plots of $\log f_{MoO_3 \cdot nH_2O}$ versus $\log f_{H_2O}$ from the data of Glemser and von Haeseler (1962) suggests that the hydration number decreases with increasing temperature (Fig. 7). This conclusion is supported by the results of similar studies of the behaviour of other metallic gas species, e.g., those of Archibald et al. (2001, 2002), who found that the hydration number of $AuCl \cdot nH_2O$ and $Cu_3Cl_3 \cdot nH_2O$ decreases from 5 to 3 and from 7.6 to 5.1 as temperature increases from 300 to 360 °C and 280 to 320 °C, respectively (see also Migdisov and Williams-Jones, 2005).

4.3. Vapour-phase Mo speciation

Although the experimental methods employed in this and previous studies cannot distinguish a monomeric from a polymeric species, studies of Mo speciation in aqueous solution have isolated only monomeric species at very low Mo concentrations ($>10^{-3}$ M; Tytko et al., 1987), so because of the low Mo concentrations in water vapour, we will assume that the monomer is the dominant gaseous species in our study. Likewise, we cannot distinguish a Mo hydroxide from a hydrate, but as there is no known stoichiometric gaseous Mo species containing more than one molecule of H_2O, we will assume that the species is hydrated.

The coordination of molybdenum may be tetrahedral or octahedral, but the coordination of gaseous species cannot be determined from solubility data, and thus it is unknown whether coordination changes or remains constant with a variation in the number of water molecules in the hydration shell. Molybdenum may have had either octahedral or tetrahedral coordination in the di- to tri-hydrate species ($MoO_3 \cdot 2–3H_2O$) interpreted from our experiments, whereas it is most likely to have been tetrahedrally coordinated in the monohydrate species of Glemser and von Haeseler (1962) and Belton and Jordan (1965), because of the very low pressures and very high temperatures employed in their experiments. An octahedral coordination of Mo in the di- to trihydrate is consistent with both crystallographic data and Mo speciation in aqueous solution. For example, a XRD study by Krebs (1972) showed that Mo in the crystal structure of $MoO_3 \cdot 2H_2O$ is coordinated to five oxygen atoms and one molecule of H_2O, which form a distorted octahedron around the metal. In this example, the second water molecule acts as hydrate water between the layers of octahedra, and is not coordinated to Mo. Molybdenum is also octahedrally coordinated in α-$MoO_3 \cdot H_2O$, in which it forms double chains of edge-sharing [$MoO_5(H_2O)$] octahedra (Boeschen and Krebs, 1974). In aqueous solution (liquid), for which the behaviour of Mo may be similar to that in the gaseous state, the metal is likewise known to form octahedral complexes. EXAFS and XANES analyses by Yokoi et al. (1993) showed that in solutions containing <3 M HCl, Mo exists as hydrates such as $MoO_2(H_2O)_4^{2+}$, in which the central Mo atom is octahedrally coordinated. Similarly, UV–visible spectroscopic analyses by Ozeki et al. (1996) showed that the dissolved structure of H_2MoO_4 is a distorted octahedron. Finally, Messaoudi et al. (2004) used density function calcu-

lations to examine the dimerization of $MoO_2(OH)(H_2O)_3^+$ to $Mo_2O_5(H_2O)_6^{2+}$ in both gas and liquid, and determined that the reactant species is most stable as an octahedron defined by the three H_2O ligands. However, tetrahedrally coordinated Mo species are also known; Mo in MoO_4^{2-} and $HMoO_4^-$ has a tetrahedral coordination in aqueous solution (Mosselmans et al., 1996; Ozeki et al., 1996). Thus, it may be possible for Mo to have both octahedral and tetrahedral coordination in the vapour phase.

4.4. Geological implications

The solubility of Mo in water vapour determined from the present study and by other experimental studies at higher temperature is many orders of magnitude higher than predicted by volatility calculations (Pankratz, 1982). This suggests that the transport of Mo by vapour in natural hydrothermal systems (e.g., porphyries) may be much more important than previously thought. As discussed by Henley and McNabb (1978), porphyry Cu–Mo systems are commonly dominated by water vapour, and thus it is reasonable to propose that vapour transport may be an important process in the formation of economic Mo porphyry deposits.

Indeed, simple calculations based on the physicochemical parameters of typical porphyry systems illustrate that vapour transport alone is sufficient for the formation of an economic deposit. Assuming that the solubility of Mo in the vapour is governed by the reaction

$$MoO_3 \cdot H_2O(g) + 2H_2S(g) \Longleftrightarrow MoS_2(s) + 3H_2O(g) + 0.5O_2(g) \quad (12)$$

and that f_{O_2} and f_{H_2S} are buffered by the assemblage hematite-magnetite-pyrite, using the thermodynamic data for $MoO_3{\cdot}H_2O$ in the JANAF tables and thermodynamic data for other species from Pankratz (1982, 1987), it can be shown that at 600 °C and 500 bars (typical P-T conditions for a porphyry system; White et al., 1981) the solubility of Mo in the vapour is 0.5 ppm. If it is further assumed that the flux of water vapour is 5 million tonnes per year (measured at actively degassing fumaroles from Satsuma–Iwojima volcano, Japan; Saito et al., 2001), then approximately 2.5 tonnes Mo would be transported and deposited annually. The formation of an economic Mo porphyry deposit, such as the Endako porphyry, British Columbia (336 Mt at 0.087% Mo), would therefore take about 115,000 years, which is within the lifetime of known geothermal systems (Silberman and White, 1975; Christiansen, 1984). A much higher solubility (perhaps as much as two orders of magnitude higher) and a much shorter time for the formation of the Endako deposit would be predicted if, as seems likely, the hydration number of the gaseous Mo species was >1. Indeed, such a prediction might be consistent with analyses showing that vapour-rich inclusions from porphyry Mo deposits can have concentrations as high as 300 ppm (Ulrich et al., 1999).

5. Conclusions

Results of our experiments show that economically significant amounts of MoO_3 can potentially be transported in water vapour, and that the solubility of MoO_3 is approximately 20 orders of magnitude higher than that predicted from volatility data. It is also evident from the results that the solubility of MoO_3 increases with increasing water fugacity, which indicates that the metal forms a gaseous hydrated complex of the type $MoO_3{\cdot}nH_2O$ by the reaction:

$$MoO_3(g) + nH_2O(g) \Longleftrightarrow MoO_3 \cdot nH_2O(g) \quad (13)$$

The hydration numbers for this species are 2.0 ± 1.0 at 300 °C, 2.4 ± 0.6 at 320 °C, and 3.1 ± 0.3 at 360 °C, and the corresponding values of $\log K$ for the formation reaction (13) are 18 ± 5 at 300 °C, 16 ± 3 at 320 °C, and 12 ± 1 at 360 °C. The log fugacity of$MoO_3{\cdot}nH_2O$ is a non-linear function of $\log f_{H_2O}$, and thus the hydration number, which is equal to the slope of the tangent line for this function, varies with water pressure. At 1 bar the hydration number is equal to ~1, and increases with increasing water pressure (2–3 at ~100 bars), although it may decrease with increasing temperature. Calculations based on the data discussed in this paper suggest that water vapour can transport Mo in sufficient concentrations for it to constitute a viable ore fluid.

Acknowledgments

The research presented in this paper was funded in part by a NSERC CRO grant to A.E.W.-J. Funding was also provided by Lynch and Leroy fellowships from McGill University, as well as a GEOTOP bursary, to K.U.R. An earlier version of this manuscript was improved by a review by C. Gammons. The current version benefited from helpful comments from three Geochimica et Cosmochimica Acta reviewers and Associate Editor J. Schott.

Associate editor: Jacques Schott

References

Anderson, G.M., Crerar, D.A., 1993. *Thermodynamics in geochemistry: the equilibrium model*. Oxford University Press, New York, NY, 588 pp.

Archibald, S.M., Migdisov, A.A., Williams-Jones, A.E., 2001. The stability of Au-chloride complexes in water vapor at elevated temperatures and pressures. *Geochim. Cosmochim. Acta* **65**, 4413–4423.

Archibald, S.M., Migdisov, A.A., Williams-Jones, A.E., 2002. An experimental study of the stability of copper chloride complexes in water vapor at elevated temperatures and pressures. *Geochim. Cosmochim. Acta* **66**, 1611–1619.

Belton, G.R., Jordan, A.S., 1965. The volatilization of molybdenum in the presence of water vapor. *J. Phys. Chem.* **69**, 2065–2071.

Boeschen, I., Krebs, B., 1974. Crystal structure of white molybdic acid, α-$MoO_3{\cdot}H_2O$. *Acta Crystallogr.* **30**, 1795–1800.

Buiten, J., 1968. Oxidation of propylene by means of SnO_2–MoO_3 catalysts: I. The effect of combining SnO_2 and MoO_3. *J. Catal.* **10**, 188–199.

Burnham, C.W., 1979. Magmas and hydrothermal fluids. In: Barnes, H.L. (Ed.), second ed., *Geochemistry of Hydrothermal Ore Deposits* Wiley, Toronto, 798 pp.

Chase, M.W., 1998. NIST-JANAF thermochemical Tables. fourth ed., J. Phys. Chem. Ref. Data, Monograph 9, 1951 pp.

Christiansen, R.L., 1984. Yellowstone magmatic evolution: its bearing on understanding large-volume explosive volcanism. In: *Studies in Geophysics: Explosive Volcanism: Inception, Evolution, and Hazards*. National Academic Press, Washington, DC, pp. 84–95.

Eastoe, C.J., 1982. Physics and chemistry of the hydrothermal system at the Pangua porphyry deposit, Bougainville, Papua New Guinea. *Econ. Geol.* **77**, 127–153.

Elliott, R.B., 1952. Gaseous hydrated oxides, hydroxides, and other hydrated molecules. PhD. Thesis, University of California, Radiation Laboratory Report 1831, 52 pp.

Glemser, O., von Haeseler, R., 1962. Gaseous hydroxides, IV: gaseous hydroxides of molybdenum and tungsten. *Z. Anorg. Allgem. Chem.* **316**, 168–181.

Heinrich, C.A., Ryan, C.G., Mernagh, T.P., Eadington, P.J., 1992. Segregation of ore metals between magmatic brine and vapor: a fluid inclusion study using PIXE Microanalysis. *Econ. Geol.* **87**, 1566–1583.

Heinrich, C.A., Günther, D., Audétat, A., Ulrich, T., Frischknecht, R., 1999. Metal fractionation between magmatic brine and vapor, determined by microanalysis of fluid inclusions. *Geology* **27**, 755–758.

Henley, R.W., McNabb, A., 1978. Magmatic vapor plumes and groundwater interaction in porphyry copper emplacement. *Econ. Geol.* **73**, 1–19.

Kestin, J., Sengers, J.V., Kamgar-Parsi, B., Levelt Sengers, J.M.H., 1984. Thermophysical properties of fluid water. *J. Phys. Chem. Ref. Data* **13**, 175–183.

Krebs, B., 1972. Crystal structure of molybdenum trioxide dihydrate. *Acta Crystallogr.* **28**, 2222–2231.

Messaoudi, S., Furet, E., Gautier, R., Le Fur, E., Pivan, J.-Y., 2004. A density functional study of the dimerization mechanisms of molybdenum(vi) in aqueous solution. *Phys. Chem.* **6**, 2083–2087.

Migdisov, A.A., Williams-Jones, A.E., 2005. An experimental study of cassiterite solubility in HCl-bearing water vapor at temperatures up to 350 °C: implications for tin ore formation. *Chem. Geol.* **217**, 29–40.

Millner, T., Neugenbauer, J., 1949. Volatility of the oxides of tungsten and molybdenum in the presence of water vapour. *Nature* **163**, 601–602.

Mosselmans, J.F.W, Schofield, P.F., Charnock, J.M., Garner, C.D., Pattrick, R.A.D., Vaughan, D.J., 1996. X-ray absorption studies of metal complexes in aqueous solution at elevated temperatures. *Chem. Geol.* **127**, 339–350.

Nadeau, O., Williams-Jones, A.E., 2004. The compositions of high-temperature fumarolic gases at Merapi volcano, Indonesia. Unpublished data.

Ozeki, T., Adachi, H., Ikeda, S., 1996. Estimation of the dissolved structures and condensation reactivities of mononuclear molybdenum(VI) species in solution using UV–vis absorption spectra and molecular orbital calculation DV-Xα. *Bull. Chem. Soc. Japan* **69**, 619–625.

Pankratz, L.B., 1982. *Thermodynamic Properties of Elements and Oxides*. United States Bureau of Mines, Bulletin 672, 509 pp.

Pankratz, L.B., Mah, A.D., Watson, S.W., 1987. *Thermodynamic Properties of Sulfides*. United States Bureau of Mines, Bulletin 689, 427 pp.

Reynolds, T.J., Beane, R.E., 1985. Evolution of hydrothermal fluid characteristics at the Santa Rita, New Mexico porphyry deposit. *Econ. Geol.* **80**, 1328–1347.

Robie, R.A., Bethke, P.M., Toulmin, M.S., Edwards, J.L., 1966. X-ray crystallography data, densities, and molar volumes of minerals. In: Clark, S.P. (Ed.), *Handbook of Physical Constants*, revised ed. GSA memoir 97, pp. 437–458.

Saito, G., Kazahaya, K., Shinohara, H., Stimac, J., Kawanabe, Y., 2001. Variation of volatile concentration in a magma system of Satsuma-Iwojima volcano deduced from melt inclusion analyses. *J. Volcanol. Geotherm. Res.* **108**, 11–31.

Sandler, S.I., 1989. *Chemical and Engineering Thermodynamics*. Wiley, New York, 622 pp..

Sardi, A., 1963. Contributions to the reduction of Mo trioxide, II. Appearance of oxides phases between Mo trioxide and Mo dioxide during reduction of Mo trioxide by a flowing gas mixture containing hydrogen and water. *Acta Chim. Acad. Sci. Hung.* **39**, 145–160.

Silberman, M.L., White, D.E., 1975. Limits on duration of hydrothermal activity at Steamboat Springs, Nevada, by K–Ar ages of spatially distributed associated altered and unaltered volcanic rocks. *Econ. Geol.* **70**, 1329.

Tytko, K.H., Baethe, G., Mehmke, K., 1987. What is "molybdic acid" or "polymolybdic acid"? *Z. Anorg. Allg. Chem.* **555**, 98–108.

Ulrich, T., Gunther, D., Heinrich, C.A., 1999. Gold concentrations of magmatic brines and the metal budget of porphyry copper deposits. *Nature* **399**, 676–679.

White, W.H., Bookstrom, A.A., Kamilli, R.J., Ganster, M.W., Smith, R.P, Ranta, D.E., Steininger, R.C., 1981. Character and origin of Climax-type molybdenum deposits. *Econ. Geol.* **75th Anniversary Volume**, 270–316.

Williams-Jones, A.E., Migdisov, A.A., Archibald, S.M., Xiao, Z., 2002. Vapor-transport of ore metals. In: Hellmann, R., Wood, S.A. (Eds.), *Water–Rock Interaction, Ore Deposits, and Environmental Geochemistry: A Tribute to David A. Crerar*. The Geochemical Society, Special Publication No. 7, pp. 279–305.

Yokoi, K., Matsubayashi, N., Miyanaga, T., Watanabe, I., Ikeda, S., 1993. Studies on the structure of molybdenum(VI) in acidic solution by XANES and EXAFS. *Polyhedron* **12**, 911–914.